Highlights on Spanish Astrophysics X, Proceedings of the XIII Scientific Meeting of the Spanish Astronomical Society held on July 16 – 20, 2018, in Salamanca, Spain. B. Montesinos, A. Asensio Ramos, F. Buitrago, R. Schödel, E. Villaver, S. Pérez-Hoyos, I. Ordóñez-Etxeberria (eds.), 2019

The Hubble constant from SN Refsdal.

J. Vega-Ferrero[1,2], J. M. Diego[2], V. Miranda[1], and G. M. Bernstein[1]

[1] Department of Physics and Astronomy, University of Pennsylvania, 209 S. 33rd St, Philadelphia, PA 19104, USA
[2] IFCA, Instituto de Física de Cantabria (UC-CSIC), Av. de Los Castros s/n, 39005 Santander, Spain

Abstract

On December 2015, Hubble Space Telescope (HST) observations detected the expected fifth counter image of SN Refsdal at $z = 1.49$. In [33], we compare the time delay predictions from numerous models with the measured value derived by [16] from very early data in the light curve of the SN Refsdal, and find a best value for $H_0 = 64^{+9}_{-11}$ km s^{-1} Mpc^{-1} (68% CL), in excellent agreement with predictions from CMB and recent weak lensing data + BAO + BBN (from the DES Collaboration). This is the first constraint on H_0 derived from time delays between multiple lensed SN images, and the first with a galaxy cluster lens, so subject to systematic effects different from other time delay H_0 estimates. Additional time delay measurements from new multiply-imaged SNe will allow derivation of competitive constraints on H_0.

1 Introduction

Galaxy clusters bend the path of photons emitted by distant objects, creating multiple images of the same background source, each with different magnification and arrival times. Time delays between multiple images of the same source depend on the cosmological model, and most notably on the Hubble constant, H_0. The potential to constrain H_0 with multiple supernova (SN) images was first suggested by [26] more than half a century ago. However, no multiply imaged (and resolved) SN has ever been observed until just recently. In 2014 four counter-images of the same supernova, SN Refsdal [15, 28, 16, 17], located at redshift $z = 1.49$, were found around a member galaxy in the cluster MACSJ1149.5+2223 (hereafter MACS1149, [7]) at redshift $z = 0.544$. The predicted time delay between these four images is relatively small (a few days) making them impractical to derive useful constraints on H_0. Approximately a year after the initial detection of the four supernova images, a fifth counter-image appeared, this one having a considerably longer time delay (see Figure 1). The

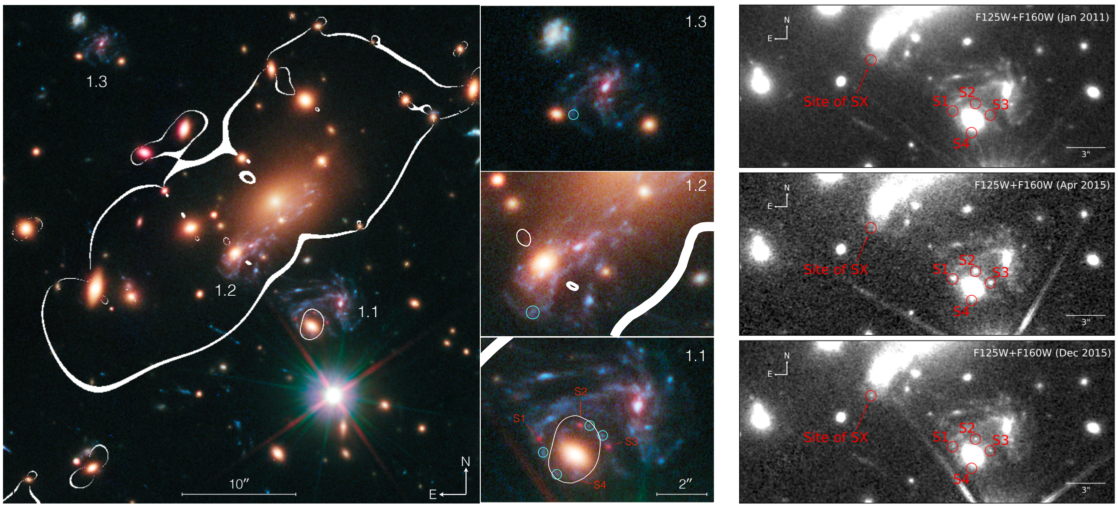

Figure 1: Left-hand panel extracted from [15]: Color-composite image of the galaxy cluster MACSJ1149. The white contours correspond to the critical curves for sources at the $z = 1.49$ (i.e., the redshift of the SN Refsdal's host galaxy). Three images of the host galaxy formed by the cluster are marked with white labels (1.1, 1.2, and 1.3) in the left panel and enlarged in the right panel. The four current images of SN Refsdal that we detected (labeled S1 to S4 in red) appear as red point sources in image 1.1. Right-hand panel extracted from [16]: images of the MACS J1149 galaxy cluster field taken with HST WFC3-IR. The top panel shows images acquired in 2011 before the SN appeared in S1–S4 or SX. The middle panel displays images taken on 2015 April 20 when the four images forming the Einstein cross are close to maximum brightness, but no flux is evident at the position of SX. The bottom panel shows images taken on 2015 December 11 which reveal the new image SX of SN Refsdal.

position and the time of reappearance were predicted by different lens models with remarkable precision [24, 30, 6, 32, 12]. This accuracy is possible since MACS1149 has been observed with unprecedented detail as part of the *Hubble Frontier Fields* program (hereafter, HFF, [21]).

The predictions for the SN time delay were based on a set of assumptions, including the value $H_0 = 70$ km s^{-1} Mpc^{-1}, which was adopted by all teams in their model predictions. Since time delays are inversely proportional to H_0, it is possible to constrain the value of H_0 directly, as originally suggested by Refsdal in 1964.

In [33], we derived an estimate of H_0 based on the observed time delay for the SN Refsdal system and an ensemble of lens models derived by different teams that use independent reconstruction methods. Our results provide a separate geometrical inference for H_0 at intermediate redshift [18, 29, 34, 3]. Hereafter, we adopt a fiducial cosmological model with $\Omega_m = 0.3$ and $\Omega_\Lambda = 0.7$, which is the cosmology used to infer the lens models. When re-scaling the value of the predicted time delay, the only cosmological parameter being changed is H_0 (see section 2 for details).

2 Hubble constant estimate from SN Refsdal time delays

The time delay Δt with respect to an unperturbed null geodesic depends on the angular separation between the image and the source, on the lensing potential at the position of the image, and on the cosmological model through the angular diameter distances. Distances, in turn, depends on the cosmic expansion history of the universe, which is proportional to the Hubble rate,

$$\Delta t(\bar{\theta}) = \frac{1+z_d}{c}\frac{D_d D_s}{D_{ds}}\left[\frac{1}{2}(\bar{\theta}-\bar{\beta})^2 - \psi(\bar{\theta})\right], \quad (1)$$

where $\bar{\beta}$ is the unlensed source position and $\psi(\bar{\theta})$ is the lens potential at the position of the observed counter-image $\bar{\theta}$. The quantities D_d, D_s and D_{ds} are the angular diameter distance to the lens, to the source and between the lens and the source, respectively. These three distances are inversely proportional to H_0, and therefore the time delay is also inversely proportional to H_0. The factor $D_d D_s/D_{ds}$ encodes the cosmological dependency that, as shown by [3], is mostly sensitive to H_0 and depends weakly on other cosmological parameters. For instance, a change of 10% in the cosmological parameter Ω_m translates into a change of only $\approx 0.1\%$ in Δt. Because of this weak dependence on other cosmological parameters, we consider the cosmological model fixed and vary only H_0. The difference in the predicted time delay between two positions in the lens plane depends on a delicate balance between the lensing potential and the relative separations. Nevertheless, the uncertainties in the lensing potential are the primary source of systematic errors in the prediction of the time delays, followed by the unknown value of H_0.

Luckily, lensing models for clusters like MACS1149 are constrained by tens of multiply-imaged lensed background galaxies with a wide range of known redshifts [9, 10, 11, 19, 35, 4, 5, 6, 14, 20, 22], reducing the uncertainties in the lens models [13, 1]. Model predictions for time delays are less prone to errors in regions where the number of lensing constraints are more abundant. In the case of MACS1149, the highest density of lensing constraints is found in the vicinity of the multiple supernova images. One should then expect systematics to be relatively small in the case of the SN Refsdal.

2.1 The case of SN Refsdal

The SN Refsdal [15, 28, 16, 17] was the first example of a resolved multiply imaged lensed SN. The first estimation of the relative time delay and magnification ratio of S1 (position of knot 1 in the original quadruplet image) and SX (the position at which SN Refsdal reappeared) based on the early light curve of SX was presented by [16] . The lensing constraints from the HFF program allowed for a variety of predictions of the time delay and relative magnification of a fifth image. These predictions where made assuming a fiducial cosmological model, needed for computing the distances in equation 1. If the fiducial model assumed the wrong H_0 this would translate into a predicted time delay that is biased with respect to the measured one. Table 1 in [33] summarizes the predicted time delays Δt_{X1} between SX and S1, and the magnification ratios, $\mu_{X1} \equiv \mu(X)/\mu(1)$, as derived by the different models presented in [32] and by the model presented in [6]. The predictions ranged from ≈ 8 months [30] to ≈ 1 year

[6]. Similar predictions extending from ≈ 7.2 months to ≈ 12.3 months were later published in [32] by different teams. SN Refsdal reappeared promptly approximately one year after its first appearance. Overall, the lens models predict reasonably well the time of reappearance of SN Refsdal [16].

Although the uncertainties in the lens models are difficult to quantify, they are generally small in regions on the lens plane where lensing constraints are abundant, as shown by [23]. In this work, as proposed by [31], we adopt a conservative level of 6% for systematic errors in the time delay predictions (see also [8] for a similar discussion). We refer the reader to section 2.1 in [33] for a detailed discussion on the model uncertainties.

The lens models assumed a fiducial Hubble constant of $H_0^{\rm fid} = 70$ km s^{-1} Mpc^{-1}, and using the lens geometry data G each modeler m derived a probability $p_m(\Delta t_{X1}, \mu_{X1}|H_0^{\rm fid}, {\rm G})$. Since the time delay is inversely proportional to H_0 as given by equation 1, we can rescale this to any alternative value of H_0 via

$$p_m(\Delta t_{X1}, \mu_{X1}|H_0, {\rm G}) = p_m\left(\frac{H_0^{\rm fid}}{H_0}\Delta t_{X1}, \mu_{X1}|H_0^{\rm fid}, {\rm G}\right). \tag{2}$$

3 Bayesian analysis

The time delays Δt_{X1} and magnifications μ_{X1} predicted by the different lens models can be compared with those inferred by [16] from the observed light curve data (LC) of both SN images. The probability $p_d(\Delta t_{X1}, \mu_{X1}|{\rm LC})$ derived by [16] shows substantial correlation between Δt_{X1} and μ_{X1} as a consequence of the incompleteness in the light curve data they analyze. By re-scaling the predictions as described in equation 2, we can infer the most likely value of H_0 that best matches the model predictions with the observations. For this purpose, we adopt a standard Bayesian approach, but keeping in mind that our observational data D are the union of lens geometry (G) and SN light curve data (LS), and both are interpreted in terms of time delay and magnification ratio. The probability of H_0 given the data D is expressed as

$$\begin{aligned} {\rm P}(H_0|{\rm D}) &\propto {\rm P}(H_0)\ {\rm P}({\rm D}|H_0) \\ &= {\rm P}(H_0)\int d\Delta t_{X1}\, d\mu_{X1}\, {\rm P}(\Delta t_{X1}, \mu_{X1}|{\rm D}, H_0){\rm P}({\rm D}) \\ &\propto {\rm P}(H_0)\int d\Delta t_{X1}\, d\mu_{X1}\ p_m(\Delta t_{X1}, \mu_{X1}|H_0, {\rm G}) \times\ p_d(\Delta t_{X1}, \mu_{X1}|{\rm LC}), \end{aligned} \tag{3}$$

where the prior, ${\rm P}(H_0)$, is the credibility of the H_0 values without the data D, and the likelihood, ${\rm P}({\rm D}|H_0)$, is the probability that the data could be generated by the models with parameter value H_0. Equation 3 is basically the product of the observed probability distribution of the observed time delay and magnification (p_d) times the probability distribution from the individual models (p_m). For a particular model, the maximum of the probability is obtained for a value of H_0 that maximizes the overlap of the SN light curve data and model probabilities.

For each individual lens model, we assume a bivariate but separable normal distribution for $p_{m,i}(\mu_{X1}, \Delta t_{X1}|H_0)$. The mean values of μ_{X1} and Δt_{X1} for each model are given in table 1 in [33] along with their statistical uncertainties. In the computation of $p_{m,i}(\mu_{X1}, \Delta t_{X1}|H_0)$, we also take into account that the statistical uncertainties are non-symmetric for three of the listed lens models. For the observational data, we associate a bivariate normal distribution to $p_d(\mu_{X1}, \Delta t_{X1})$ based on the best-fit ellipse to the 68% CL in Figure 3 of [16] (for brevity, we drop the dependences on G and LC from our notation). Both $p_{m,i}(\mu_{X1}, \Delta t_{X1}|H_0)$ and $p_d(\mu_{X1}, \Delta t_{X1})$ are normalized to unity. Note that $p_m(\mu_{X1}, \Delta t_{X1}|H_0)$ depends on H_0 as defined in equation 2. On the contrary, the probability distribution of the observational data, $p_d(\mu_{X1}, \Delta t_{X1})$, does not depend on H_0.

We adopt two strategies for combining the probabilities p_m derived by different lens models, which we can label by $i = 1 \ldots M$. A very optimistic view is that each model has errors that are independent and are drawn from an ensemble with zero mean. In this case, we can set

$$p_m(\Delta t_{X1}, \mu_{X1}|H_0) \propto \prod_{i=1}^{M} p_i(\Delta t_{X1}, \mu_{X1}|H_0), \tag{4}$$

and we will label the resultant posterior derived from equation 3 as $\mathrm{P}_\times(H_0|\mathrm{D})$. A more conservative (and more realistic) assumption is that only one of the models is correct, with prior probability q_i that model i is the one. In this case, we have

$$p_m(\Delta t_{X1}, \mu_{X1}|H_0) = \sum_{i=1}^{M} q_i p_i(\Delta t_{X1}, \mu_{X1}|H_0). \tag{5}$$

We will assign equal priors $q_i = 1/M$ to each model, such that we effectively average the probabilities of the models, and denote the resultant posterior distribution as $\mathrm{P}_+(H_0|\mathrm{D})$. Note that the models do not contribute equally to the posterior: those whose predictions of μ_{X1} disagree with the measurements of [16] will be downweighted in the integral of equation 3.

4 Results and conclusions

In the left-hand panel in figure 2, we show the contribution from each model to the total posterior $\mathrm{P}_+(H_0|\mathrm{D})$ using a flat prior for H_0 between $H_0 = 30$ and 100 km s^{-1} Mpc^{-1}. The right-hand panel in figure 2 summarizes our main result for the posterior $\mathrm{P}_\times(H_0|\mathrm{D})$ and $\mathrm{P}_+(H_0|\mathrm{D})$. We have assumed that all model predictions are equal prior validity (but see [23] for a comparison of the performance of the different lensing reconstruction techniques). The median value and 68% CL for H_0 are: $H_0 = 62^{+4}_{-4}$ km s^{-1} Mpc^{-1} for the $\mathrm{P}_\times(H_0|\mathrm{D})$ posterior; and $H_0 = 64^{+9}_{-11}$ km s^{-1} Mpc^{-1} for the $\mathrm{P}_+(H_0|\mathrm{D})$ posterior. These values of H_0 already include a systematic uncertainty at the 6% level which has been added at the end in quadrature to the statistical uncertainty.

We constrain, for the first time, the Hubble constant following Refsdal's original idea to use a multiple-lensed SN with measured time delays and precise lens model predictions. By combining the results of multiple lens models, we account for statistical and some systematic

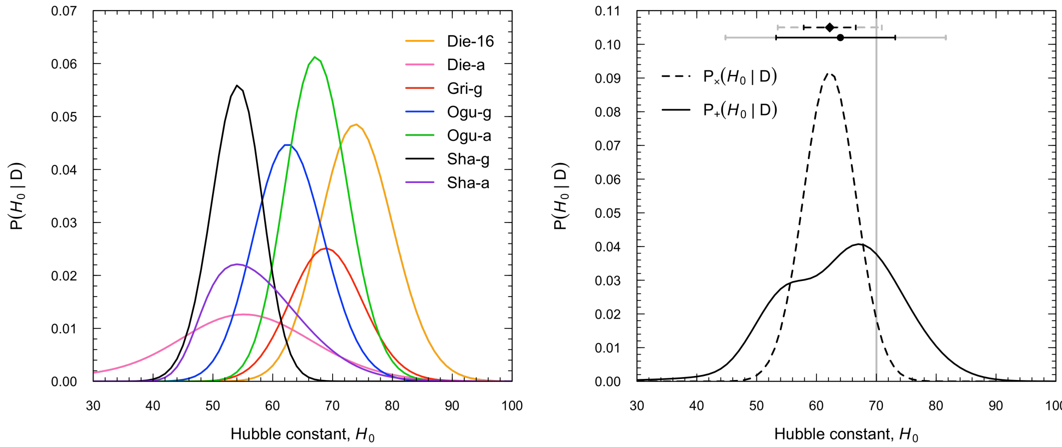

Figure 2: Left-hand panel extracted from [33]: Contribution of each lens model prediction (in different colors) to the posterior $P_+(H_0|D)$ obtained by equation 3. Right-hand panel extracted from [33]: Total posterior $P_\times(H_0|D)$ (dashed line) and $P_+(H_0|D)$ (solid line). Both curves include a systematic uncertainty at the 6% level added at the end in quadrature to the statistical uncertainty. We explicitly show the median, 68% CL (black error bars) and 95% CL (grey error bars) on the top of the figure for both posteriors. The vertical line corresponds to the fiducial $H_0^{\rm fid} = 70$ km s^{-1} Mpc^{-1} assumed in all the lens models.

errors due to assumptions made during the lens reconstruction. These results are in good agreement with recent constraints from CMB, LSS, and local distance ladders [25, 27, 2]. We use a very weak prior to better show the sensitivity of the Refsdal data to the parameter H_0. Future improved constraints on the observed time delay and magnification will reduce the uncertainty in the Hubble parameter using this technique, and additional estimates derived from different clusters will provide a competitive test for H_0.

Acknowledgments

We thank P.L. Kelly and D. Scolnic for feedback helpful discussions. J.V-F and G.M.B. acknowledge support from the Space Telescope Science Institute (contract number 49726). J.M.D. acknowledges the support of projects AYA2015-64508-P (MINECO/FEDER, UE), AYA2012-39475-C02-01, and the consolider project CSD2010-00064 funded by the Ministerio de Economía y Competitividad. J.V-F and J.M.D. acknowledge the hospitality of the University of Pennsylvania. V.M. was supported in part by the Charles E. Kaufman Foundation.

References

[1] Acebron, A., Jullo, E., Limousin, M., et al. 2017, MNRAS, 470, 1809

[2] Abbott, T. M. C., Abdalla, F. B., Annis, J., et al. 2018, MNRAS, 480, 3879

[3] Bonvin, V., Courbin, F., Suyu, S. H., et al. 2017, MNRAS, 465, 4914

[4] Diego, J. M., Broadhurst, T., Molnar, S. M., Lam, D., & Lim, J. 2015a, MNRAS, 447, 3130

[5] Diego, J. M., Broadhurst, T., Zitrin, A., et al. 2015b, MNRAS, 451, 3920

[6] Diego, J. M., Broadhurst, T., Chen, C., et al. 2016, MNRAS, 456, 356

[7] Ebeling, H., Edge, A. C., & Henry, J. P. 2001, ApJ, 553, 668

[8] Greene, Z. S., Suyu, S. H., Treu, T., et al. 2013, ApJ, 768, 39

[9] Jauzac, M., Jullo, E., Eckert, D., et al. 2015a, MNRAS, 446, 4132

[10] Jauzac, M., Jullo, E., Eckert, D., et al. 2015b, MNRAS, 446, 4132

[11] Jauzac, M., Richard, J., Jullo, E., et al. 2015c, MNRAS, 452, 1437

[12] Jauzac, M., Richard, J., Limousin, M., et al. 2016, MNRAS, 457, 2029

[13] Johnson, T. L., & Sharon, K. 2016, ApJ, 832, 82

[14] Kawamata, R., Oguri, M., Ishigaki, M., Shimasaku, K., & Ouchi, M. 2016, ApJ, 819, 114

[15] Kelly, P. L., Rodney, S. A., Treu, T., et al. 2015, Science, 347, 1123

[16] Kelly, P. L., Rodney, S. A., Treu, T., et al. 2016a, ApJ Letters, 819, L8

[17] Kelly, P. L., Brammer, G., Selsing, J., et al. 2016b, ApJ, 831, 205

[18] Kundić, T., Turner, E. L., Colley, W. N., et al. 1997, ApJ, 482, 75

[19] Lam, D., Broadhurst, T., Diego, J. M., et al. 2014, ApJ, 797, 98

[20] Limousin, M., Richard, J., Jullo, E., et al. 2016, A&A, 588, A99

[21] Lotz, J. M., Koekemoer, A., Coe, D., et al. 2017, ApJ, 837, 97

[22] Mahler, G., Richard, J., Clément, B., et al. 2018, MNRAS, 473, 663

[23] Meneghetti, M., Natarajan, P., Coe, D., et al. 2017, MNRAS, 472, 3177

[24] Oguri, M. 2015, MNRAS, 449, L86

[25] Planck Collaboration, Ade, P. A. R., Aghanim, N., et al. 2016, A&A, 594, A13

[26] Refsdal, S. 1964, MNRAS, 128, 307

[27] Riess, A. G., Macri, L. M., Hoffmann, S. L., et al. 2016, ApJ, 826, 56

[28] Rodney, S. A., Strolger, L.-G., Kelly, P. L., et al. 2016, ApJ, 820, 50

[29] Sereno, M., & Paraficz, D. 2014, MNRAS, 437, 600

[30] Sharon, K., & Johnson, T. L. 2015, ApJ Letters, 800, L26

[31] Suyu, S. H., Auger, M. W., Hilbert, S., et al. 2013, ApJ, 766, 70

[32] Treu, T., Brammer, G., Diego, J. M., et al. 2016, ApJ, 817, 60

[33] Vega-Ferrero, J., Diego, J. M., Miranda, V., & Bernstein, G. M. 2018, ApJ Letters, 853, L31

[34] Wong, K. C., Suyu, S. H., Auger, M. W., et al. 2017, MNRAS, 465, 4895

[35] Zitrin, A., Zheng, W., Broadhurst, T., et al. 2014, ApJ Letters, 793, L12